

# Semi-Automated Segmentation of Pelvic Organs for AR Guided Robotic Prostatectomy

Wenzhe Shi\*, Lin Mei\*, Ara Darzi, and Philip Edwards\*

Dept. of Biosurgery and Surgical Technology Imperial College London, UK  
ws207,l.mei,eddie.edwards@imperial.ac.uk

**Abstract.** Building subject-specific 3D models for pelvic organs from preoperative imaging is a vital step in achieving augmented reality guidance for robotic prostatectomy. This paper presents a semi-automatic method for calculating deformations from atlas models to subject specific models for pelvis, lower spine, coccyx, rectum and prostate. The method consists of three stages and requires no more than 5 minutes human intervention in identifying 31 landmarks located in the lower abdominal region. The first step is to perform point-based affine and non-rigid registration to produce an initial deformation for the whole pelvic region. The second step refine this deformation with two levels of intensity-based non-rigid registration, the result of which is then used as the input to third stage where organ-specific deformations are produced by non-rigid registrations applied to the region of interest. We applied this method to build subject-specific models for 18 patients. When compared with manual segmentation produced by expert clinicians, the result showed around 20% improvement over the baseline method, which uses only intensity-based affine and non-rigid registration, and more than 90% on some case where the baseline method failed. We believe this is a significant step towards clinically usable segmentation of lower abdominal organs for augmented reality guided robotic prostatectomy.

## 1 Introduction

Prostate cancer is an increasing problem in an aging society. Amongst the possible treatments, minimally invasive robotic radical prostatectomy is rapidly gaining acceptance [1]. There are, however, significant rates of incontinence, impotence or incomplete resection [2]. It is crucial that the surgeon accurately targets the prostate, particularly near the prostatic apex, and that the surrounding neuro-vascular bundle is well preserved.

These difficulties can be eased using intraoperative image guidance. It is suggested that augmented reality (AR) provides better guidance through improved visualisation [3]. AR technology overlays the 3D models of important structures onto surgeon's field of view. The fact that Da Vinci system uses a real-time stereo video captured by endoscope as surgeon's view makes it a natural platform for implementing AR guidance.

One major step towards AR surgical guidance is to build patient-specific 3D models of the important organs located in the operational region. These

models are normally built by segmentation of preoperative images such as MRI and CT. Segmentation is a huge research field. One option is the use of an atlas. A template segmentation can be registered to an individual, which has been applied to segmentation of brain [4] and lung tissues[5]. Segmentation of kidneys has been proposed using a gradient-fitting deformable atlas [6], and also segmentation of other abdominal organs such as liver, kidneys, and spinal cord using a thin-plate spline based probabilistic atlas [7].

Research in segmentation of the prostate and surrounding pelvic organs is driven mainly by demand in radiotherapy. Intensity-based methods are proposed for MRI [8, 9]. A statistical atlas has also been proposed. Shen et. al. built a statistical shape model from ultrasound images [10]. Arambula proposed an active shape model that is optimised by a genetic algorithm [11]. Pasquier et. al. compared a seed growing method to an adaptive atlas based on morphological filtering for the prostate and other abdominal organs on MRI. They found atlas-based segmentation to be more robust but it requires minor interactive corrections, while region-growing only works fine for the bladder and rectum, for which MRI shows good soft-tissue contrast [12]. Their model is further extended to a probabilistic atlas which deforms only along a certain principle modes in the training set [13].

To calculate the deformation that warps an atlas to a specific image, one can use a direct search along the degrees of freedom(DOF) of the atlas. This method allows unrealistic deformation to be introduced due to unwanted local maxima. A possible enhancement is to train a statistical atlas which only deforms within a feasible shape space. However, this enhancement requires a significant training set. Otherwise restricted deformation may result in failed segmentation for uncommon shapes in the presence of pathology.

In this paper we present a semi-automatic segmentation-by-registration scheme for building models of pelvic organs including lower spine, coccyx, rectum including rectal-sigmoid junction, and prostate. The original atlas is built on visible human (VH) [14], and the targeted images are preoperative MR scans of 18 patients. Despite varying resolution, different MR sequences and pathological shape variation, our method still managed to produce feasible segmentation after minor manual corrections.

## 2 Method

Segmentation by registration has been proposed for the lung [5]. Since this method does not restrict atlas deformation, it can be used for segmenting pathological images. A hierarchy of affine and non-rigid registration proposed by Rueckert et. al. [15] is used to calculate the transformation that warps the atlas 3D model to fit the subject's anatomy.

The non-rigid transformation is described by a regular grid of 3D control points. The B-spline interpolates the displacements inbetween the control points. The displacement of a control point only affects its local neighbourhood. Hence a single b-spline transformation can represent both local and global deformation.

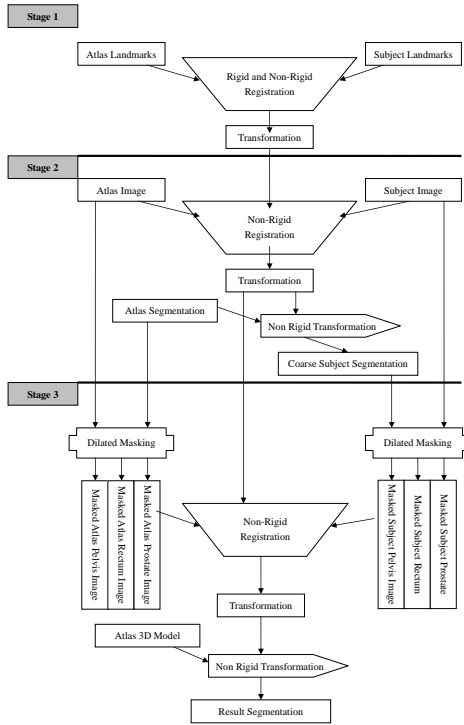


**Fig. 1.** Flow chart of the registration process

Also, since the atlas remains the same, the control points of transformation for different individuals naturally correspond. Such correspondence is a requirement for statistical shape analysis.

In order to produce an accurate transformation, the hierarchical registration consists of three stages - landmark based registration, intensity-based coarse registration and a series of registrations performed for each organ (see Fig. 1). Note that the direction of registration is in fact from subject to atlas because the resulting transformation calculates the corresponding points in the source image space for a target image voxel.

## 2.1 Stage I: Landmark-based Registration

Corresponding landmarks are manually selected in the atlas and the subject images. This provides an initial registration. A total of 31 landmarks are used: 18 on the pelvis, 2 on either end of the rectum and 11 on the prostate. The selection of the landmarks on the pelvis and rectum avoids common misregistrations

resulting from the intensity based approach. The selection of the landmarks on prostate is to cope with some extremely pathological shape variation.

Affine registration is performed on the landmarks to align the position and orientation. This is followed by a non-rigid registration using 20mm grid size of which the output transformation is applied to the subject image to produce a starting point for the next stage. We will describe the reason for choosing this grid size in the following section.

## 2.2 Stage II: Intensity-Based Hierarchical Non-Rigid Registration

The second stage is to perform a series of non-rigid registrations between the atlas and subject's MR scans. T2-weighted MRI is used because it is one of the most commonly used diagnostic images and has better soft tissue contrast than CT or T1-weighted MRI and because the central gland and peripheral zone are distinguishable [16]. This makes it possible to produce a detailed segmentation of the prostate.

The registration uses a B-spline as the non-rigid transformation and normalised mutual information (NMI) as the similarity measure. NMI is selected since it is proven to be the most effective similarity measures for registration of between images with different modalities [17, 18].

After applying the resulting transformation of stage I onto the subject's image, an intensity-based non-rigid registration is performed.

Since displacing the control points would only affect their neighbourhoods and the smoothness of the local deformation is affected by control point spacing, larger spacing leads to a smoother and more global deformation while a relatively smaller spacing leads to a more localised but less smooth deformation. The nature of the gradient descent optimisation approach with NMI gives rise to slow convergence properties and increased sensitivity to local minima. These unattractive features are especially evident when trying to align large and complex images. One standard enhancement is a hierarchical approach.

The basic idea is to start with a coarse initial grid size and sub-sampled image, and refine the transformation iteratively with increasing image resolution and decreasing grid size. In our experiments we increase image resolution and reduce the grid size both by a factor of two at each iteration. A large grid size is required to avoid a highly localised deformation. However, when grid size is too large, there will be more than one landmark in one grid cell and the b-spline function fails to interpolate their displacement. It was found that when grid size is too large, the result of stage I may not be sufficiently accurate.

Taking into account the trade-off between avoiding a very localised deformation and providing interpolation of the dense landmarks on the prostate, the settings in table 1 are used:

## 2.3 Stage III: Registration on the Region of Interest

A mask of the atlas is created for each organ by dilating the binary segmentation. This provides a greyscale image that includes the organ and some surrounding

|           | Coarse Level                         | Refined Level                        |
|-----------|--------------------------------------|--------------------------------------|
| Stage I   | 20mm grid size with 5mm voxel size   | N/A                                  |
| Stage II  | 20mm grid size with 5mm voxel size   | 10mm grid size with 2.5mm voxel size |
| Stage III | 10mm grid size with 2.5mm voxel size | 5mm grid size with 1.25mm voxel size |

**Table 1.** Grid size with corresponding voxel size

tissue. Separate images are created for the pelvis (including partial spine and coccyx), the rectum, and the prostate. This reduces the unwanted influence of tissues more distant from the target organs. This also speeds up the registration process, allowing smaller grid size and voxel dimension to be used.

In the last stage, we apply the resulting transformation from stage II to the subject's image and register it onto each masked atlas respectively to get the transformation for each organ. Applying these transformations to the 3D model built from atlas segmentation we get the subject specific model.

### 3 Experiment and Results

#### 3.1 Atlas Construction and Subject Image Preprocessing

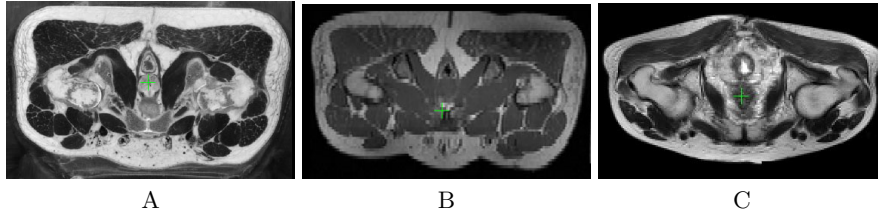


**Fig. 2.** Visible Human images: Cryo-section (A), T-1 MRI (B) and a combined MRI of a subject(C).

We used the Visible Human (VH) cryo-sectional image for manual segmentation because it provides good visualisations of the pelvic soft tissues (see figure 2). The pelvis is segmented and registration performed using the VH T1 MRI because of poor soft-tissue contrast in CT and poor image quality for T2 MRI.

We acquired lower abdomen MRI scans for 18 patients. There are multiple scans per subject, generally 5mm axial and sagittal slices with high in-plane resolution ( $0.8mm \times 0.8mm$ ) together with a few focused T2 scans of the prostate providing higher resolution. In order to take advantage of all these images, we resample to the highest resolution and calculate a weighted average image that is used for registration. An example is shown in figure 2 C.

The segmentation procedure described in section 2 is used to propagate the manual segmentation to all the subjects. Since the modality of VH MRI and the patients' MRIs are very different, we chose the patient with the best registration

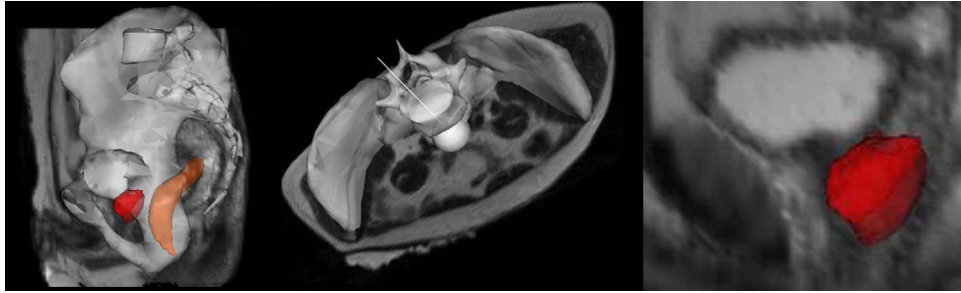


**Fig. 3.** An example of the segmented subject model.

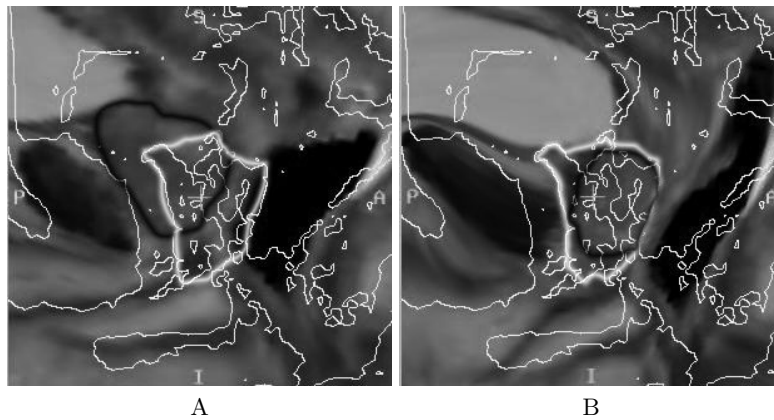


**Fig. 4.** Segmentation of prostates (marked with bright rings) using direct intensity-based registration (A) and using landmark(B) before intensity-based registration. The true prostate positions are marked by dark rings

result to use as the atlas and propagate this segmentation result to its peers. Results are shown below in section 3.2.

### 3.2 Segmentation by Registration

Figure 3 shows an example of patient specific model. We compared the result of our method with a baseline method using the direct intensity-based affine registration followed by two levels of non-rigid registration.

Figure 4 shows results with and without landmark guidance are compared, and figure 5, shows results with and without a masked atlas are compared. Dramatic improvement in accuracy are found in both.

Quantitative evaluation is done by comparing the results to manual segmentation produced for 4 subjects by clinicians. Using normalised partition distance [19] as measure, our method showed around 35% improvement over the baseline, and significant improvement (more than 90%) on some case where simple intensity-based registration failed(see table 2).

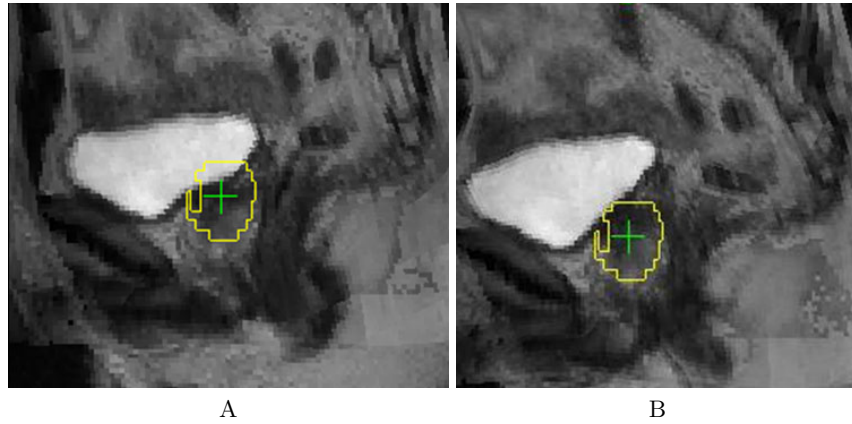


**Fig. 5.** Segmentation of prostates (marked with bright rings) without using masked atlas (A) and using masked atlas(B).

|           | Patient 003 | Patient 005 | Patient 007 | Patient 008 |
|-----------|-------------|-------------|-------------|-------------|
| Baseline  | 9.0%        | 49.1%       | 3%          | 2.2%        |
| Stage I   | 10.4%       | 10.2%       | 6.4%        | 3.5%        |
| Stage II  | 7.3%        | 7.4%        | 5.9%        | 2.5%        |
| Stage III | 4.9%        | 4.2%        | 4.5%        | 1.8%        |

**Table 2.** Example partition distances (in voxels) between the manual gold standard and the semi-automatic segmentation after each registration step.

## 4 Discussion

We proposed a useful hierarchical segmentation-by-registration scheme for pelvic organs. Compared to manual segmentation, improvement is found at each stage. Possible further developments include automatic landmark identification and construction of a statistical shape or deformation model to restrict the degrees of freedom of the transformation.

## References

1. El-Hakim, A., Tewari, A.: Robotic prostatectomy – a review. *MedGenMed* **6** (2004) 20
2. Kaul, S., Savera, A., Badani, K., Fumo, M., Bhandari, A., Menon, M.: Functional outcomes and oncological efficacy of vattikuti institute prostatectomy with veil of aphrodite nerve-sparing: an analysis of 154 consecutive patients. *BJU Int.* **97** (2006) 467–472
3. Nowinski, W.: Virtual reality in brain intervention: models and applications. *Engineering in Medicine and Biology Society, 2005. IEEE-EMBS 2005. 27th Annual International Conference of the (Jan. 2005)* 4164–4167

4. Cuadra, M., Pollo, C., Bardera, A., Cuisenaire, O., Villemure, J.G., Thiran, J.P.: Atlas-based segmentation of pathological mr brain images using a model of lesion growth. *Medical Imaging, IEEE Transactions on* **23**(10) (Oct. 2004) 1301–1314
5. Sluimer, I., Prokop, M., vanGinneken, B.: Toward automated segmentation of the pathological lung in ct. *Medical Imaging, IEEE Transactions on* **24**(8) (Aug. 2005) 1025–1038
6. Gao, L.M., Heath, D.G., Fishman, E.K.: Abdominal image segmentation using three-dimensional deformable models. *Invest. Radiol.* **33** (1998) 348–355
7. Park, H., Bland, P., Meyer, C.: Construction of an abdominal probabilistic atlas and its application in segmentation. *Medical Imaging, IEEE Transactions on* **22**(4) (April 2003) 483–492
8. Chiu, B., Freeman, G., Salama, M., Fenster, A., Rizkalla, K., Downey, D.: A segmentation algorithm using dyadic wavelet transform and discrete dynamic contour. *Electrical and Computer Engineering, 2003. IEEE CCECE 2003. Canadian Conference on* **3** (May 2003) 1481–1484
9. Samiee, M., Thomas, G., Fazel-Rezai, R.: Semi-automatic prostate segmentation of mr images based on flow orientation. *Signal Processing and Information Technology, 2006 IEEE International Symposium on* (Aug 2006) 203–207
10. Shen, D., Zhan, Y., Davatzikos, C.: Segmentation of prostate boundaries from ultrasound images using statistical shape model. *Medical Imaging, IEEE Transactions on* **22**(4) (April 2003) 539–551
11. Cosío, F.A. In: *Prostate Segmentation Using Pixel Classification and Genetic Algorithms*. Springer Berlin / Heidelberg (2005) 910–917
12. Pasquier, D., Lacornerie, T., Vermandel, M., Rousseau, J., Lartigau, E., Betrouni, N.: Segmentation of prostate boundaries from ultrasound images using statistical shape model. *International Journal of Radiation Oncology Biology Physics* **68**(2) (April 2007) 592–600
13. Betrouni, N., Puech, P., Dewalle, A., Lopes, R., Dubois, P., Vermandel, M.: 3d automatic segmentation and reconstruction of prostate on mr images. *Engineering in Medicine and Biology Society, 2007. EMBS 2007. 29th Annual International Conference of the IEEE* (Aug. 2007) 5259–5262
14. Spitzer, V., Ackerman, M., Scherzinger, A., Whitlock, D.: The visible human male: atechanical report. *Journal of the American Medical Informatics Association* **3**(2) (1996) 118–30
15. Rueckert, D., Sonoda, L.I., Hayes, C., Hill, D.L.G., Leach, M.O., Hawkes, D.J.: Nonrigid registration using free-form deformations: Application to breast mr images. *IEEE Trans. Med. Imag.* **18**(18) (Aug 1996) 712–721
16. Mattson, J., Simon, M.: *The Pioneers of NMR and Magnetic Resonance in Medicine: The Story of MRI*. Jericho & New York: Bar-Ilan University Press (1996)
17. Pennney, G., Weese, J., Little, J., Desmedt, P., Hill, D., Hawkes, D.: A comparison of similarity measures for use in 2-d-3-d medical image registration. *Medical Imaging, IEEE Transactions on* **17**(4) (Aug 1998) 586–595
18. Zitova, B., Flusser, J.: Image registration methods: a survey. *Image and Vision Computing* **21**(11) (October 2003) 977–1000
19. Cardoso, J., Corte-Real, L.: Toward a generic evaluation of image segmentation. *Image Processing, IEEE Transactions on* **14**(11) (Nov. 2005) 1773–1782